

DeepInit Phase Retrieval

Martin Reiche and Peter Jung

Abstract—This paper shows how data-driven deep generative models can be utilized to solve challenging *phase retrieval* problems, in which one wants to reconstruct a signal from only few intensity measurements. Classical iterative algorithms are known to work well if initialized close to the optimum but otherwise suffer from non-convexity and often get stuck in local minima. We therefore propose *DeepInit Phase Retrieval*, which uses regularized gradient descent under a deep generative data prior to compute a *trained* initialization for a fast classical algorithm (e.g. the randomized Kaczmarz method). We empirically show that our hybrid approach is able to deliver *very high* reconstruction results at low sampling rates even when there is significant generator model error. Conceptually, learned initializations may therefore help to overcome the non-convexity of the problem by starting classical descent steps closer to the global optimum. Also, our idea demonstrates superior runtime performance over conventional gradient-based reconstruction methods. We evaluate our method for generic measurements and show empirically that it is also applicable to diffraction-type measurement models which are found in terahertz single-pixel phase retrieval.

I. INTRODUCTION

An important nonlinear inverse problem is the *phase retrieval* problem, which has been extensively studied over the last decades because it arises in a lot of applications, e.g. crystallography (Harrison, 1993)(Millane, 1990), astronomy (Fienup and Dainty, 1987) and (optical) imaging (Shechtman et al., 2014). It was originally formulated as the problem of reconstructing a signal from the magnitude of its Fourier transform which, for example, arises when illuminating a scene with a coherent electromagnetic field and measuring its magnitude in the far field. A classical alternating recovery approach here is the well-known *Fienup algorithm* (Fienup, 1982) which iteratively imposes real-plane and Fourier-plane constraints.

A related variant of the aforementioned problem is the reconstruction of the scene from its diffraction pattern. Diffraction occurs when a wave hits an obstacle (whose size is in the order of the wavelength) or passes an aperture, and therefore influences its complex-valued wave pattern. Since most detectors can only measure intensity, phase retrieval techniques are necessary to recover the original signal. For example, in single-detector imaging a target scene is repeatedly illuminated with radiation that has passed a spatial light modulator configured with a random on/off pixel pattern. The modulated radiation pattern then hits the scene and its transmission is collected through a collecting optics (e.g. a lens) at a single detector cell. With an accurate forward diffraction model it is possible to computationally recover the scene from the collected intensity measurements (computational imaging).

An important aspect to improve recovery and reduce acquisition time is to incorporate prior knowledge about targets in the scene. For example, an intuitive assumption

is that the signals may be (approximately) represented as sparse vectors in some known transform domain. However, in many applications sparsity is often a too simple description of realistic signal structures. Therefore, a more recent approach is to learn the signal structure directly from training data. Neural networks can be trained to denoise desired signals while *generative neural networks* can learn a particular source characteristics. Not surprisingly, a lot of prior research has been conducted at the intersection of deep learning and nonlinear inverse problems.

In a more generic formulation of phase retrieval, one wants to find an n -dimensional signal vector \mathbf{x} such that the vector $|\mathbf{Ax}|^2$ of intensities is consistent with an observation vector $\mathbf{y} \in \mathbb{R}_+^m$ where $\mathbf{A} \in \mathbb{C}^{m \times n}$ is a given complex-valued measurement (or sensing) matrix (modeling the wave propagation in the diffraction imaging example mentioned above). In practice one always has to consider measurement noise due to non-optimal detectors and then a particularly simple approach is to formulate recovery for example as:

$$\min_{\mathbf{x}} \|\mathbf{y} - |\mathbf{Ax}|^2\|_2^2 \quad (1)$$

Given a more concrete noise model, other loss functions are also feasible for applications. A fundamental question however is when a signal is uniquely (up to trivial ambiguities) determined by noiseless intensity measurements. For example, Eldar and Mendelson have shown that for $m = \mathcal{O}(n)$ subgaussian measurements the problem has with overwhelming probability a unique (up to its sign) solution (Eldar and Mendelson, 2014). The precise scaling has a longer history, see for example (Bandeira et al., 2014). Further uniqueness results exist, e.g., in the case of random binary matrices, see (Krahmer and Liu, 2018; Krahmer and Stöger, 2019).

Besides identifiability it is important for applications to solve the problem also with robust and computationally tractable algorithms obeying rigorous guarantees. Fienup’s algorithm is known to be very efficient but is not guaranteed to recover the correct solution (Osherovich, 2012). On the other hand, semidefinite relaxations like *PhaseLift* (Candes et al., 2011) yield a convex problem for which rigorous guarantees exist. But such lifting approaches are extremely computationally demanding and are therefore more of theoretical than of practical use.

To overcome computational burden, gradient descent based approaches for the nonconvex loss function have been investigated intensively. For example, Candes et al. proposed a *Wirtinger Flow* approach (Candes et al., 2015) that aims to minimize the intensity loss $\|\mathbf{y} - |\mathbf{Ax}|^2\|_2^2$. This method was extended to use truncated gradients (Chen and Candes, 2015) which converge faster to the optimal value. Wang et al. proposed *Truncated Amplitude Flow* (Wang et al., 2016) which minimizes the amplitude

loss $\|\sqrt{y} - |\mathbf{A}\mathbf{x}|\|_2^2$. Especially for real-valued signals, Tan and Vershynin proposed a very fast *randomized Kaczmarz* approach by iteratively choosing one of the measurements $\sqrt{y_i} = |\langle \mathbf{a}_i, \mathbf{x} \rangle|$ at random and projecting onto the closer of the two hyperplanes corresponding to $\pm \mathbf{x}$ (Tan and Vershynin, 2017).

However, since all these iterative approaches operate on non-convex loss functions, careful initialization is necessary in practice. In real world imaging applications it is important to have an initialization which is also close to the optimum so that descent algorithms run into the correct local minima. This is exactly a point where learning may help in classical algorithms. For example, autoencoders can be used as trainable denoisers to improve reconstruction when used as regularizers or proximal mappings in iterative algorithms. For example, *prDeep* (Metzler et al., 2018) is based on the regularization by denoising (RED) approach (Romano et al., 2017) to minimize the amplitude-based objective function by adding a generative neural network-based denoiser regularization term (they used the well-known *DnCNN* (Zhang et al., 2017) network).

II. DEEPINIT PHASE RETRIEVAL

As indicated above, prior information about permissible signals \mathbf{x} may drastically improve the reconstruction for phase retrieval algorithms. In particular, generative models based on deep (feed-forward) neural networks are interesting as they are able to learn to generate samples even from very complicated signal distributions (such as e.g. natural images (Gulrajani et al., 2016) or faces (Karras et al., 2018)).

Using a deep generative model as a prior follows the idea that we have given a generator $G : \mathbb{R}^p \rightarrow \mathbb{R}^n$ for $p \ll n$ that has been trained to sufficiently well generate permissible signals. Instead of reconstructing a signal \mathbf{x}^* directly, one considers then (in the case of intensity loss as data fidelity):

$$\min_{\mathbf{z}} \|\mathbf{y} - |\mathbf{A}G(\mathbf{z})|\|_2^2 + \lambda R(\mathbf{z}) \quad (2)$$

where $R : \mathbb{R}^p \rightarrow \mathbb{R}_+$ is a given regularizer function. Obviously, due to the quadratic measurements and the nature of G the objective above is non-convex and can usually be minimized only locally using descent methods and a good initialization. A point \mathbf{z}^* in the latent space obtained in this way yields then a reconstruction $G(\mathbf{z}^*) = \mathbf{x}^*$ (same for other loss functions, like the amplitude loss). In the case of linear measurements and for $\lambda = 0$, this approach has been investigated in (Bora et al., 2017) as a data-driven extension of compressed sensing.

In (Hand et al., 2018) it has been proven that for differentiable generator networks consisting of layers with ReLU activation functions and Gaussian \mathbf{A} , the unregularized ($\lambda = 0$) objective function in (2) does (with overwhelming probability) not have spurious local minima away from neighborhoods of the true solution (or negative multiples thereof). An analogous proof has been provided for the linear case already in (Hand and Voroninski, 2017) including a Tikhonov regularization term $R(\mathbf{z}) = \|G(\mathbf{z})\|_2^2$. Asim et al. experimentally validated an approach to solve

a regularized linear case with $R(\mathbf{z}) = \|\mathbf{z}\|_2$ using L-BFGS with great success on important computer vision datasets where G was trained to operate on normal distribution in the latent space (Asim et al., 2019). Further works by (Shamshad and Ahmed, 2018) and (Hand et al., 2018) propose to minimize the (unregularized) amplitude loss $\|\sqrt{y} - |\mathbf{A}G(\mathbf{z})|\|_2^2$ with a gradient descent scheme.

In this work we will consider TV-regularized phase retrieval with $R(\mathbf{z}) = \|G(\mathbf{z})\|_{\text{TV}}$ in (2), i.e., for a given generator G the problem is:

$$\min_{\mathbf{z}} \|\mathbf{y} - |\mathbf{A}G(\mathbf{z})|\|_2^2 + \lambda \|G(\mathbf{z})\|_{\text{TV}} \quad (3)$$

where $\|\cdot\|_{\text{TV}}$ is the *discrete anisotropic total variation norm*. In the linear case such a regularized approach has been investigated already in (Ulyanov et al., 2020) and with additionally learned regularizers in (Van Veen et al., 2018). Formulation (3) is especially beneficial when the generator has not been properly trained and therefore yields notable residual model error $\min_{\mathbf{z}} \|\mathbf{x} - G(\mathbf{z})\|$. Problem (3) can be solved using (sub-)gradient descent. However, since the optimization (3) in terms of $\mathbf{x} = G(\mathbf{z})$ is limited to the range of the generator, the achieved performance will depend critically on the quality of G and how representative the training data is for the target to recover.

Deep Generative Initialization

Given the shortcomings of the deep generative prior-based reconstruction methods described above with respect to the generator’s model error, we propose to use a hybrid approach that takes the reconstruction result of a generative prior-based method and uses that as initialization for a classical algorithm. Conceptually, this works as follows: First we reconstruct an approximate $\tilde{\mathbf{x}} = G(\tilde{\mathbf{z}})$ using a randomly initialized sub-gradient descent for problem (3). We call this step “Deep Regularized Gradient Descent” (DRGD). As we have discussed, the similarity of $\tilde{\mathbf{x}}$ to the true \mathbf{x} is depending on the generator G ’s ability to correctly model the signal domain. Then we use $\tilde{\mathbf{x}} = G(\tilde{\mathbf{z}})$ as initialization $\mathbf{x}^{(0)}$ for a traditional reconstruction method in order to solve (1). Doing this, we overcome the model error of the generator G but are still able to use the prior knowledge encoded into it without compromising reconstruction quality.

Our hypothesis is that based on this data-driven initialization $\mathbf{x}^{(0)}$ of the reconstruction method, we get better reconstruction results as we start closer to the true value of \mathbf{x} . We furthermore need potentially less iterations to get to comparable reconstruction errors. In comparison to the spectral initialization method employed by most reconstruction methods, our initialization method is also significantly faster. Figure 1 shows comparisons of both initialization methods with respect to runtime.

Below, we investigate our hybrid approach exemplary for the combination of the Deep Regularized Gradient Descent (DRGD) for (3) and the Randomized Kaczmarz (RK) algorithm for (1), which we will name *DeepInit Phase Retrieval* (DeepInit). The pseudocode is shown in Algorithm 1. We will evaluate its performance in Section III.

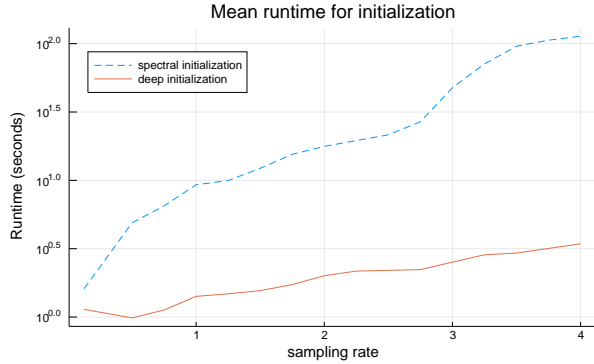


Fig. 1. Comparison of the runtime of spectral initialization against deep generative initialization. Note the logarithmic scale on the vertical axis. All results are averaged over five different images.

Algorithm 1: DeepInit Phase Retrieval algorithm

Data: measurements $\mathbf{y} = [y_1, \dots, y_m]^\top \in \mathbb{R}^m$
 sensing matrix $\mathbf{A} = [\mathbf{a}_1, \dots, \mathbf{a}_m]^\top \in \mathbb{C}^{m \times n}$
 differentiable generator network
 $G(\mathbf{z}) : \mathbb{R}^p \rightarrow \mathbb{R}^n$
 step size η
 regularization parameter λ
 number of iterations of the initializer i_{\max}
 number of iterations of the randomized
 Kaczmarz method k_{\max}

Result: reconstruction $\mathbf{x}^{(k_{\max})}$
 Randomly initialize $\mathbf{z}^{(0)} \in \mathbb{R}^p$

for $i = 0$ **to** $i_{\max} - 1$ **do**
 $\mathbf{z}^{(i+1)} \leftarrow \mathbf{z}^{(i)} -$
 $\eta \nabla_{\mathbf{z}^{(i)}} (\|\mathbf{y} - |\mathbf{A}G(\mathbf{z}^{(i)})|^2\|_2^2 + \lambda \|G(\mathbf{z}^{(i)})\|_{\text{TV}})$
end
 $\mathbf{x}^{(0)} \leftarrow G(\mathbf{z}^{(i_{\max})})$

for $k = 0$ **to** $k_{\max} - 1$ **do**
 $\mathbf{x}^{(k+1)} \leftarrow \mathbf{x}^{(k)} +$
 $\left(\frac{\text{sign}(\langle \mathbf{a}_{r(k+1)}, \mathbf{x}^{(k)} \rangle) \sqrt{y_{r(k+1)} - \langle \mathbf{a}_{r(k+1)}, \mathbf{x}^{(k)} \rangle}}{\|\mathbf{a}_{r(k+1)}\|_2} \right) \mathbf{a}_{r(k+1)}$
end

III. NUMERICAL EXPERIMENTS

In this section we will present a numerical evaluation of the proposed methods for complex Gaussian, i.e., unstructured measurements. We compare our approach against traditional phase retrieval methods (Wirtinger Flow (WF), Truncated Wirtinger Flow (TWF), and Randomized Kaczmarz (RK)) on one standard test dataset and one synthetically generated dataset using structural similarity index (SSIM) and peak signal-to-noise ratio (PSNR), two important quality metrics commonly used for image quality evaluation tasks.

A. MNIST dataset

We evaluate the performance of the reconstruction methods on the well-known MNIST dataset (LeCun, 1998) consisting of 60,000 handwritten digits represented as 28×28 pixel grayscale images. For DRGD and DeepInit, we train a variational autoencoder on this dataset. The architecture of the model can be seen in Figure 2. We use

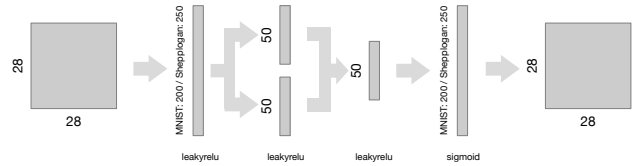


Fig. 2. Architecture of the variational autoencoder trained on MNIST and the Shepp-Logan dataset.

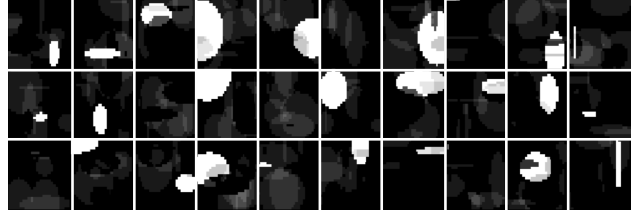


Fig. 3. 30 samples taken from the synthetically generated Shepp-Logan dataset.

an ℓ^2 -regularized ELBO as the loss function and train for 50 epochs in batches of 128 images.

B. Shepp-Logan dataset

This synthetically generated dataset is inspired by the well-known Shepp-Logan phantom by randomizing the location and size parameters of its constituent shapes. As in the MNIST dataset, each image of the Shepp-Logan dataset is 28×28 pixels in size and grayscale. The overall dataset (see Figure 3) contains 250,000 randomly generated images.

Analog to the MNIST dataset, we train a variational autoencoder using the Shepp-Logan dataset with the same loss function, batch size and epoch count that we used for the MNIST dataset. We adapt the network design of the variational autoencoder slightly as shown in Figure 2.

C. Numerical Experiments

All evaluations are performed under a noise-free measurement model $\mathbf{y} = |\mathbf{A}\mathbf{x}|^2$ using complex random Gaussian measurement matrices \mathbf{A} . We evaluate the methods based on their reconstruction quality and runtime and set their parameters as follows: Wirtinger Flow (WF) uses $k_{\max} = 50$ iterations; Truncated Wirtinger Flow (TWF) uses $k_{\max} = 200$ iterations; Randomized Kaczmarz (RK) uses $k_{\max} = 100000$ iterations;¹ Deep Regularized Gradient Descent (DRGD) uses $k_{\max} = 200$ iterations with step size $\eta = 0.1$ and regularization factor $\lambda = 0.1$; DeepInit Phase Retrieval uses $i_{\max} = 200$ iterations for the initializer with step size $\eta = 0.1$ and regularization factor $\lambda = 0.1$, and $k_{\max} = 100000$ as the iteration count for the Randomized Kaczmarz part.

Figures 5 and 6 visually show the reconstruction results for selected images from the MNIST and Shepp-Logan datasets and highlight the most important results. Figures 7 to 8 show the evaluation results with respect to reconstruction quality under SSIM and PSNR.

¹Note that Randomized Kaczmarz, unlike Wirtinger Flow or Truncated Wirtinger Flow, is not a gradient-based method and that iteration counts therefore are not comparable. In general, Randomized Kaczmarz iterations are much faster to execute than gradient steps.

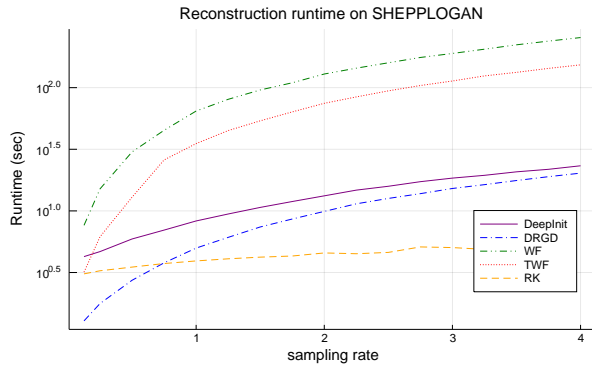


Fig. 4. Evaluation results for the MNIST and Shepp-Logan datasets with respect to the reconstruction time. Note the log scale of the vertical axis. All results are averaged over five different images.

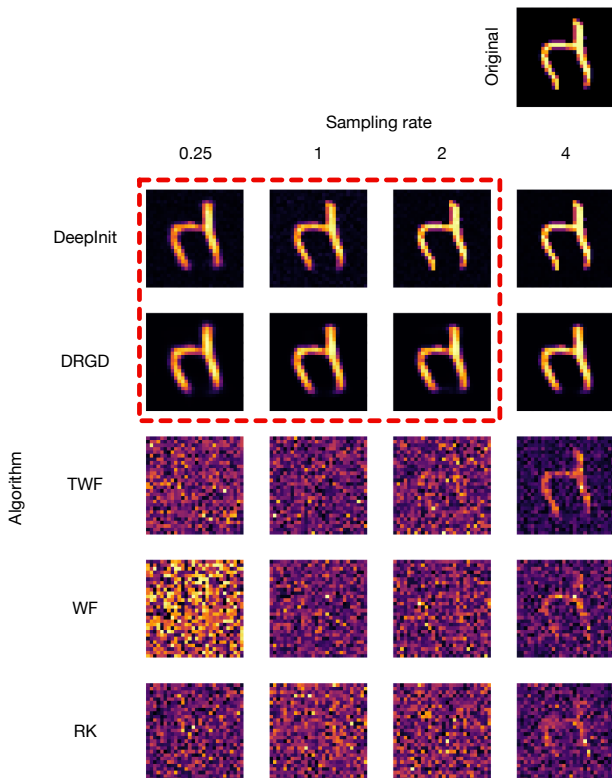


Fig. 5. Results of the reconstruction process for a selected MNIST test image for all algorithms and selected sampling rates. Deep Regularized Gradient Descent and DeepInit Phase Retrieval make use of a trained variational autoencoder. Important results are highlighted with a dashed red box.

D. Main findings and observations

1) *Reconstruction quality*: One can see that for the evaluated sampling rate range (0.125 to 4.0), DeepInit Phase Retrieval and Deep Regularized Gradient Descent show superior reconstruction quality over Truncated Wirtinger Flow, Wirtinger Flow and Randomized Kaczmarz for both evaluation data sets.

At a sampling rate of 4.0, the reconstruction quality of DeepInit Phase Retrieval is marginally lower compared to Truncated Wirtinger Flow. This effect can be attributed to the fixed number of randomized Kaczmarz iterations in the experiment and is especially visible in the results with respect to PSNR.

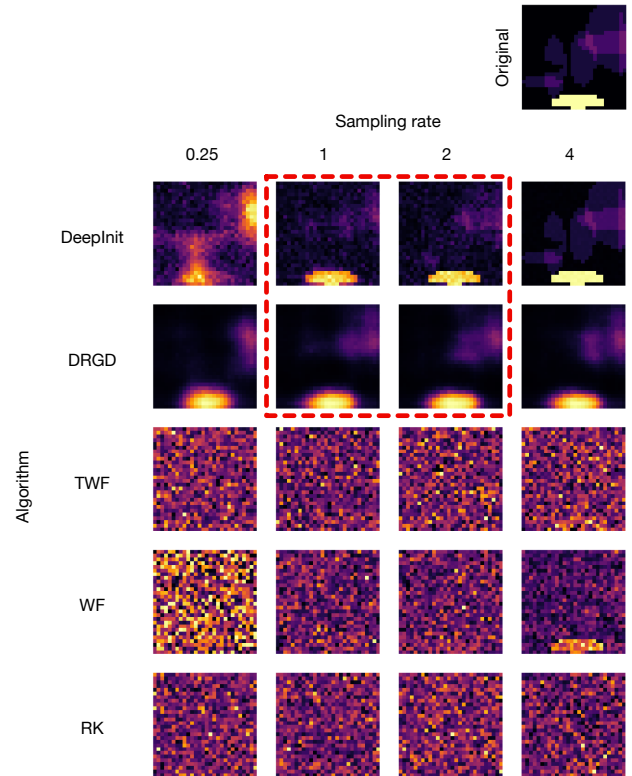


Fig. 6. Results of the reconstruction process for a selected Shepp-Logan test image for all algorithms and selected sampling rates. Deep Regularized Gradient Descent and DeepInit Phase Retrieval make use of a trained variational autoencoder. One can see that Deep Regularized Gradient Descent is unable to perform a good reconstruction due to an inability of the variational autoencoder to model the original signal distribution well enough. Important results are highlighted with a dashed red box.

Because it only allows solutions that lie in the range of the generator, Deep Regularized Gradient Descent fails to deliver competitive reconstruction results due to an inability of the variational autoencoder to model the original signal distribution well enough. This effect is not visible in reconstructions using the DeepInit Phase Retrieval algorithm, because in this method the final solution is not bound to lie in the range of the generator network.

2) *Runtime*: Our evaluation shows that DeepInit Phase Retrieval and Deep Regularized Gradient Descent both have drastically superior runtime performance when compared to Truncated Wirtinger Flow or Wirtinger Flow (see Figure 4).

IV. DEEPINIT PHASE RETRIEVAL FOR DIFFRACTION SINGLE-PIXEL IMAGING

So far we have discussed deeply initialized phase retrieval algorithms from a generic point of view for complex Gaussian intensity measurements. In this section we shall consider now a practical application of the proposed algorithms for *single-pixel imaging device*. In the optical realm, the compressive “single-pixel camera” has gained a lot of interest in research and practical applications in the last decade (Baraniuk, 2007) (Duarte et al., 2008). Such an approach allows to image a scene using only one single detector (instead of a 2D detector array as is usual in most optical systems, for example in digital cameras). In particular for imaging applications outside the visible spectrum, there are many reasons why choosing only a

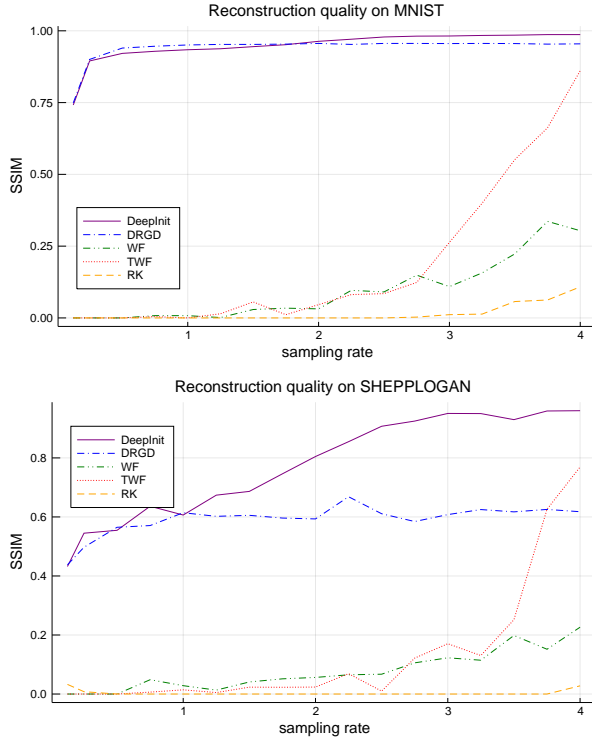


Fig. 7. Evaluation results for the MNIST and Shepp-Logan datasets with respect to the structural similarity index for image quality. All results are averaged over five different images. Note that the reconstruction quality of DeepInit Phase Retrieval is upper-bounded by a fixed number of Kaczmarz iterations.

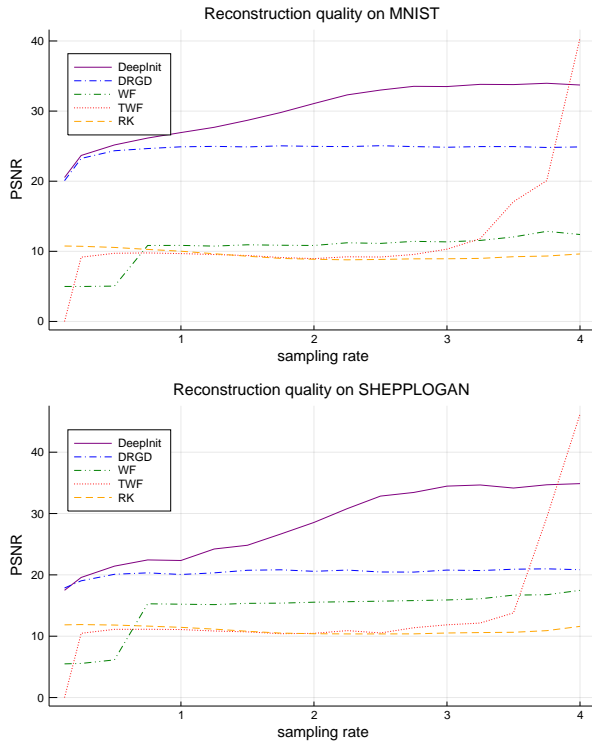


Fig. 8. Evaluation results for the MNIST and Shepp-Logan datasets with respect to the peak signal-to-noise ratio. All results are averaged over five different images. Note that the reconstruction quality of DeepInit Phase Retrieval is upper-bounded by a fixed number of Kaczmarz iterations, which is visible by the quality plateau that the algorithm reaches.

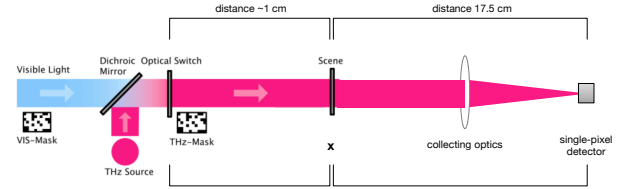


Fig. 9. Schematic view of the experimental setup. The optical switch is controlled by visible light and allows the transmission of the terahertz radiation at the parts of the mask which are set to 1, thereby imposing the pattern on the transmitted terahertz radiation. The terahertz pattern is propagated to the scene x and its transmission is collected using a collecting optics that focuses the radiation onto a single detector cell. Figure adapted from work by Augustin et al. (Augustin et al., 2017).

single detector might be advantageous: detectors might be very expensive and building an array of them might not be economically reasonable, or building a detector array might not be technically feasible due to the degree of miniaturization that would be needed for a practical application. A concrete example here is terahertz imaging which is of special interest in many different applications as terahertz radiation is non-ionizing and at the same time able to penetrate many non-conducting materials.

Our sketched application follows the system setup from (Augustin et al., 2017). We are interested in reconstructing the transmission of a scene illuminated with terahertz radiation (at a wavelength of 0.856nm , which equals to approximately 0.35THz). However, since we restrict ourselves to only have a single detector cell, we illuminate the scene with a *random* but *known* radiation pattern and collect the transmission radiation through a collecting optics (e.g. a lens) which focuses the transmitted radiation into a single detector cell that is able to measure the intensity (i.e. squared amplitude) of the incoming radiation. This process is repeated with multiple different patterns to obtain multiple measurements, which are then used to reconstruct the original signal. Figure 9 shows a schematic view of the experimental setup.

The random radiation patterns are achieved by the usage of so-called *masks* applied by a spatial light modulator (also called optical switch), a special device that modulates a radiation beam in a way that it only allows radiation to pass through at certain selectable areas (which are defined by the masks). The masks are 2-dimensional patterns represented as binary vectors $\mathbf{a}_i \in \{0, 1\}^n$.

Every electromagnetic wave is subject to diffraction effects when propagating through space after hitting an obstacle or propagating through an aperture in the size similar to its wavelength. In the optical regime these diffraction effects are negligible for many practical applications due to the extremely short wavelength of the visible light. However, in our setup, we will assume our target of interest to be of a size that is similar to the wavelength, especially will we assume that the pixel size of the image of the scene that we want to recover is approximately equal to the wavelength of the radiation.

Technically, this means that we will have to model the diffraction effects taking place between the spatial light modulator and the scene and between the scene and the detector. Diffraction effects between the terahertz source and

the spatial light modulator can be neglected as the radiation can be seen as coherent. We use the ‘‘Discrete Diffraction Transformation’’, introduced in (Katkovnik et al., 2009) and (Katkovnik et al., 2008), to approximate the diffraction by complex matrices depending on the wavelength, the propagation distance and the pixel sizes at the planes before and after the propagation. For THz imaging via phase retrieval this has already been investigated in (Burger et al., 2019).

More precisely, we model diffraction effects between the spatial light Modulator and the Scene using a diffraction matrix $D_{M \rightarrow S} \in \mathbb{C}^{n \times n}$ generated according to the simplified construction method in (Katkovnik et al., 2009) by assuming a propagation distance of 1cm (according to the system setup in Figure 9), and 28×28 quadratic pixels of edge size 0.5mm (both before and after the propagation) at a wavelength of $0.856 \cdot 10^{-3}$ m. We define a second diffraction matrix, modeling the effects between the Scene and the Detector, $D_{S \rightarrow D} \in \mathbb{C}^{n \times n}$ and will generate it analogously assuming a propagation distance of 17.5cm.

A. Diffraction Imaging Measurement Model

For our simulation, we will model the measurement at the detector as follows: a uniform illumination $[1, \dots, 1]^T$ hits the spatial light modulator which applies the mask \mathbf{a}_i . After that, the wave propagates from the spatial light modulator to the scene while being subject to diffraction $D_{M \rightarrow S}$ before it hits the scene \mathbf{x} and propagates further from the scene to the detector being subject to diffraction $D_{S \rightarrow D}$. At the detector it is summed up and its intensity is measured, leading to the following (noise-free) signal model:

$$\begin{aligned} y_i &= \left| \sum_{j=1}^n (D_{S \rightarrow D} \text{diag}(\mathbf{x}) D_{M \rightarrow S} \mathbf{a}_i)_j \right|^2 \\ &= \left| \langle \overline{D_{M \rightarrow S} \text{diag}(\mathbf{a}_i)} D_{S \rightarrow D}^H [1, \dots, 1]^T, \mathbf{x} \rangle \right|^2 \\ &=: |\langle \tilde{\mathbf{a}}_i, \mathbf{x} \rangle|^2 \end{aligned} \quad (4)$$

for the phase retrieval optimization problem (3), i.e., $\tilde{\mathbf{a}}_i$ is the i th row of the complex-valued measurement matrix \mathbf{A} in (3).

Note that this imaging problem is especially sensitive to changes of the distance between the spatial light modulator and the scene $D_{M \rightarrow S}$ (also referred to as the *stand-off distance*), because the masks commanded at the spatial light modulator drastically degrade while propagating to the scene (see Figure 10). This is caused by the diffraction matrix $D_{M \rightarrow S}$ losing rank with increasing propagation distance (an effect that is covered in more detail in (Katkovnik et al., 2009)). This results in a blurring effect, which, depending on the distance, can be up to a degree that the original signal can no longer be recovered. We will therefore investigate the reconstruction quality with respect to sensitivity to changes in the distance between the spatial light modulator and the scene for simulated data. A similar problem has been investigated experimentally in (Augustin et al., 2019).

B. Sensitivity Analysis

We investigate the sensitivity of the reconstruction quality for different stand-off distances and sampling

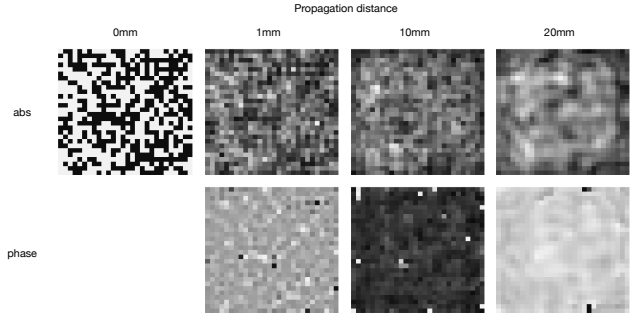


Fig. 10. Commanded Bernoulli mask (0mm) and degraded masks after 1mm, 10mm and 20mm of simulated free-space propagation.

rates $\frac{m}{n}$. Our evaluation will be done for both traditional (Truncated Wirtinger Flow) as well as deep generative prior-supported reconstruction algorithms (Deep Regularized Gradient Descent and DeepInit Phase Retrieval, both using the variational autoencoders defined in Sections III-A and III-B as their underlying generative models) and will be executed on both the MNIST dataset as well as on the synthetic Shepp-Logan dataset. To obtain reasonable results for the Truncated Wirtinger Flow algorithm, we use parameters ($a_z^{\text{lb}} = 0.001$, $a_z^{\text{ub}} = 500$) different to the usual defaults in (Chen and Candes, 2015). Figures 11 and 12 visually show the results of the reconstruction process for selected MNIST and Shepp-Logan samples for stand-off distances between 0.00125m and 0.08m.

approaches and can prove valuable in real-world physical image reconstruction problems where diffraction effects occur.

V. CONCLUSION

This work explored how deep generative models can support solving phase retrieval problems. Recent works approach solutions in the range of a trained generator network, but suffer from poor reconstruction quality when the generator is not properly able to model the signal domain. *DeepInit Phase Retrieval* also incorporates signal domain information using deep generative priors but does not suffer from reconstruction quality degradation caused by generator model error. This is because the data prior is used only during the initialization while the actual reconstruction is performed using classical algorithms like Randomized Kaczmarz iterations. Our work empirically shows that *DeepInit Phase Retrieval* achieves better reconstruction quality than provided by traditional methods at sampling rates below 4 and even comes with improved runtime compared to other gradient descent methods. For the practically motivated application in terahertz single-pixel imaging, we experimentally showed that *DeepInit Phase Retrieval* achieves reconstruction quality that is superior to Truncated Wirtinger Flow, indicating that it is well suited for real-world scenarios where diffraction plays an important role.

Acknowledgements: We thank Sven Augustin and Lukas Nickel. PJ has been supported by DFG grant JU 2795/3.

REFERENCES

M. Asim, A. Ahmed, and P. Hand. Invertible generative models for inverse problems: mitigating representation

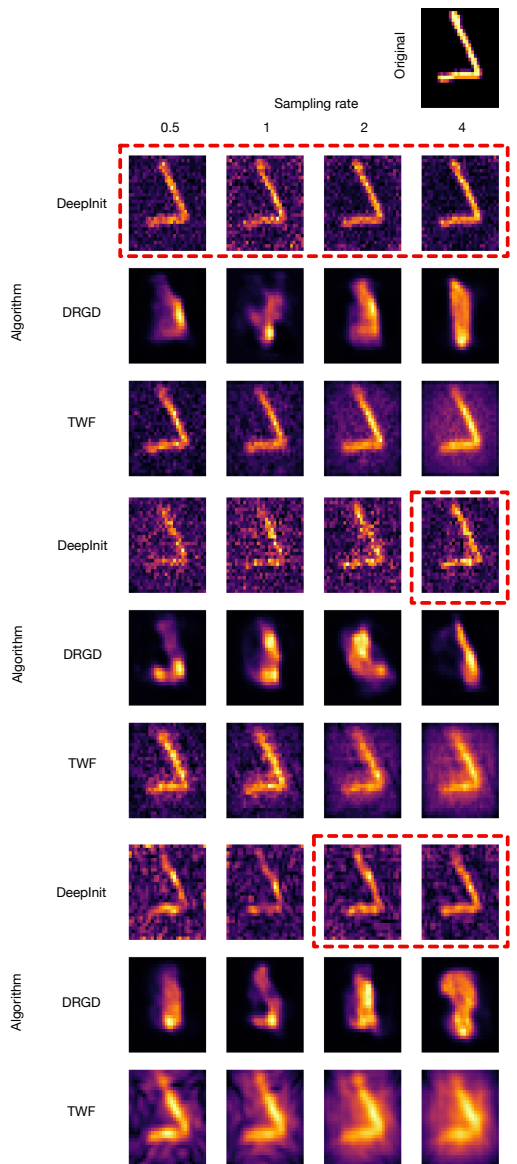


Fig. 11. Results of the reconstruction process for a selected MNIST test image for selected sampling rates at 0.125cm, 0.5cm and 2cm stand-off distances. Important results are highlighted with a dashed red box.

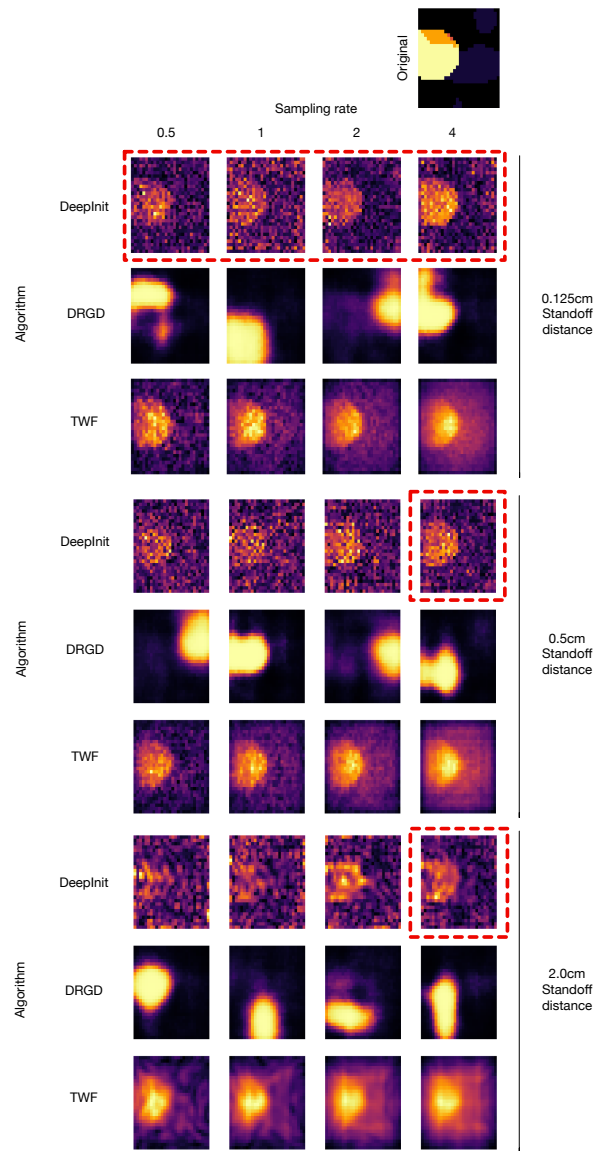


Fig. 12. Results of the reconstruction process for a sample from the Shepp-Logan dataset for selected sampling rates at 0.125cm, 0.5cm and 2cm stand-off distances. Important results are highlighted with a dashed red box.

error and dataset bias. *arXiv:1905.11672 [cs]*, May 2019. URL <http://arxiv.org/abs/1905.11672>. arXiv: 1905.11672.

- S. Augustin, S. Frohmann, P. Jung, and H.-W. Hubers. An optically controllable 0.35 THz single-pixel camera for millimeter resolution imaging. In *2017 42nd International Conference on Infrared, Millimeter, and Terahertz Waves (IRMMW-THz)*, pages 1–2, Cancun, Mexico, Aug. 2017. IEEE. ISBN 978-1-5090-6050-4. doi: 10.1109/IRMMW-THz.2017.8066996. URL <http://ieeexplore.ieee.org/document/8066996/>.
- S. Augustin, P. Jung, S. Frohmann, and H.-W. Huebers. Terahertz dynamic aperture imaging at stand-off distances using a Compressed Sensing protocol. *arXiv:1902.07935 [physics]*, Feb. 2019. URL <http://arxiv.org/abs/1902.07935>. arXiv: 1902.07935.
- A. S. Bandeira, J. Cahill, D. G. Mixon, and A. A. Nelson. Saving phase: Injectivity and stability for phase retrieval. *Applied and Computational Harmonic Analysis*, 37(1):

106–125, July 2014. ISSN 10635203. doi: 10.1016/j.acha.2013.10.002. URL <https://linkinghub.elsevier.com/retrieve/pii/S1063520313000936>.

- R. G. Baraniuk. Compressive sensing. *IEEE signal processing magazine*, 24(4), 2007. doi: 10.1109/MSP.2007.4286571. URL <https://ieeexplore.ieee.org/document/4286571>.
- A. Bora, A. Jalal, E. Price, and A. G. Dimakis. Compressed Sensing using Generative Models. *arXiv:1703.03208 [cs, math, stat]*, Mar. 2017. URL <http://arxiv.org/abs/1703.03208>. arXiv: 1703.03208.
- M. Burger, J. Föcke, L. Nickel, P. Jung, and S. Augustin. Reconstruction Methods in THz Single-pixel Imaging. *arXiv:1903.08893 [math]*, Mar. 2019. URL <http://arxiv.org/abs/1903.08893>. arXiv: 1903.08893.
- E. J. Candes, T. Strohmer, and V. Voroninski. PhaseLift: Exact and Stable Signal Recovery from Magnitude Measurements via Convex Programming. *arXiv:1109.4499 [cs, math]*, Sept. 2011. URL <http://arxiv.org/abs/1109.4499>.

- arXiv: 1109.4499.
- E. J. Candes, X. Li, and M. Soltanolkotabi. Phase Retrieval via Wirtinger Flow: Theory and Algorithms. *IEEE Transactions on Information Theory*, 61(4):1985–2007, Apr. 2015. ISSN 0018-9448, 1557-9654. doi: 10.1109/TIT.2015.2399924. URL <http://ieeexplore.ieee.org/lpdocs/epic03/wrapper.htm?arnumber=7029630>.
- Y. Chen and E. J. Candes. Solving Random Quadratic Systems of Equations Is Nearly as Easy as Solving Linear Systems. *arXiv:1505.05114 [cs, math, stat]*, May 2015. URL <http://arxiv.org/abs/1505.05114>. arXiv: 1505.05114.
- M. F. Duarte, M. A. Davenport, D. Takhar, J. N. Laska, T. Sun, K. F. Kelly, and R. G. Baraniuk. Single-pixel imaging via compressive sampling. *IEEE Signal Processing Magazine*, 25(2):83–91, Mar. 2008. ISSN 1053-5888. doi: 10.1109/MSP.2007.914730. URL <http://ieeexplore.ieee.org/document/4472247/>.
- Y. C. Eldar and S. Mendelson. Phase retrieval: Stability and recovery guarantees. *Applied and Computational Harmonic Analysis*, 36(3):473–494, May 2014. ISSN 10635203. doi: 10.1016/j.acha.2013.08.003. URL <https://linkinghub.elsevier.com/retrieve/pii/S1063520313000717>.
- C. Fienup and J. Dainty. Phase retrieval and image reconstruction for astronomy. In *Image Recovery: Theory and Application*, pages 231–275. Academic Press, 1987. ISBN 0-12-663940-X.
- J. R. Fienup. Phase retrieval algorithms: a comparison. *Applied Optics*, 21(15):2758, Aug. 1982. ISSN 0003-6935, 1539-4522. doi: 10.1364/AO.21.002758. URL <https://www.osapublishing.org/abstract.cfm?URI=ao-21-15-2758>.
- I. Gulrajani, K. Kumar, F. Ahmed, A. A. Taiga, F. Visin, D. Vazquez, and A. Courville. PixelVAE: A Latent Variable Model for Natural Images. *arXiv:1611.05013 [cs]*, Nov. 2016. URL <http://arxiv.org/abs/1611.05013>. arXiv: 1611.05013.
- P. Hand and V. Voroninski. Global Guarantees for Enforcing Deep Generative Priors by Empirical Risk. *arXiv:1705.07576 [cs, math]*, May 2017. URL <http://arxiv.org/abs/1705.07576>. arXiv: 1705.07576.
- P. Hand, O. Leong, and V. Voroninski. Phase Retrieval Under a Generative Prior. In S. Bengio, H. Wallach, H. Larochelle, K. Grauman, N. Cesa-Bianchi, and R. Garnett, editors, *Advances in Neural Information Processing Systems 31*, pages 9136–9146. Curran Associates, Inc., 2018. URL <http://papers.nips.cc/paper/8127-phase-retrieval-under-a-generative-prior.pdf>.
- R. W. Harrison. Phase problem in crystallography. *Journal of the Optical Society of America A*, 10(5):1046, May 1993. ISSN 1084-7529, 1520-8532. doi: 10.1364/JOSAA.10.001046. URL <https://www.osapublishing.org/abstract.cfm?URI=josaa-10-5-1046>.
- T. Karras, S. Laine, and T. Aila. A Style-Based Generator Architecture for Generative Adversarial Networks. *arXiv:1812.04948 [cs, stat]*, Dec. 2018. URL <http://arxiv.org/abs/1812.04948>. arXiv: 1812.04948.
- V. Katkovnik, J. Astola, and K. Egiazarian. Discrete diffraction transform for propagation, reconstruction, and design of wavefield distributions. *Applied Optics*, 47(19):3481, July 2008. ISSN 0003-6935, 1539-4522. doi: 10.1364/AO.47.003481. URL <https://www.osapublishing.org/abstract.cfm?URI=ao-47-19-3481>.
- V. Katkovnik, A. Migukin, and J. Astola. Backward discrete wave field propagation modeling as an inverse problem: toward perfect reconstruction of wave field distributions. *Applied Optics*, 48(18):3407–3423, 2009. URL http://www.cs.tut.fi/~lasip/DDT/MATRIX_DDT.pdf.
- F. Kraemer and Y.-K. Liu. Phase Retrieval Without Small-Ball Probability Assumptions. *IEEE Transactions on Information Theory*, 64(1):485–500, Jan. 2018. ISSN 0018-9448, 1557-9654. doi: 10.1109/TIT.2017.2757520. URL <http://arxiv.org/abs/1604.07281>. arXiv: 1604.07281.
- F. Kraemer and D. Stöger. Complex phase retrieval from subgaussian measurements. *arXiv:1906.08385 [cs, math, stat]*, June 2019. URL <http://arxiv.org/abs/1906.08385>. arXiv: 1906.08385.
- Y. LeCun. The MNIST database of handwritten digits, 1998. URL <http://yann.lecun.com/exdb/mnist/>.
- C. A. Metzler, P. Schniter, A. Veeraraghavan, and R. G. Baraniuk. prDeep: Robust Phase Retrieval with a Flexible Deep Network. *arXiv:1803.00212 [cs, stat]*, Feb. 2018. URL <http://arxiv.org/abs/1803.00212>. arXiv: 1803.00212.
- R. P. Millane. Phase retrieval in crystallography and optics. *JOSA A*, 7(3):394–411, 1990. URL http://xrm.phys.northwestern.edu/research/pdf_papers/1990/millane_josaa_1990.pdf.
- E. Osherovich. Numerical methods for phase retrieval. *arXiv:1203.4756 [astro-ph, physics:physics]*, Mar. 2012. URL <http://arxiv.org/abs/1203.4756>. arXiv: 1203.4756.
- Y. Romano, M. Elad, and P. Milanfar. The Little Engine That Could: Regularization by Denoising (RED). *SIAM Journal on Imaging Sciences*, 10(4):1804–1844, Jan. 2017. ISSN 1936-4954. doi: 10.1137/16M1102884. URL <https://epubs.siam.org/doi/10.1137/16M1102884>.
- F. Shamshad and A. Ahmed. Robust Compressive Phase Retrieval via Deep Generative Priors. *arXiv:1808.05854 [cs, stat]*, Aug. 2018. URL <http://arxiv.org/abs/1808.05854>. arXiv: 1808.05854.
- Y. Shechtman, Y. C. Eldar, O. Cohen, H. N. Chapman, J. Miao, and M. Segev. Phase Retrieval with Application to Optical Imaging. *arXiv:1402.7350 [cs, math]*, Feb. 2014. URL <http://arxiv.org/abs/1402.7350>. arXiv: 1402.7350.
- Y. S. Tan and R. Vershynin. Phase Retrieval via Randomized Kaczmarz: Theoretical Guarantees. *arXiv:1706.09993 [cs, math, stat]*, June 2017. URL <http://arxiv.org/abs/1706.09993>. arXiv: 1706.09993.
- D. Ulyanov, A. Vedaldi, and V. Lempitsky. Deep Image Prior. *International Journal of Computer Vision*, mar 2020. ISSN 0920-5691. doi: 10.1007/s11263-020-01303-4. URL <http://arxiv.org/abs/1711.10925><http://dx.doi.org/10.1007/s11263-020-01303-4><http://link.springer.com/10.1007/s11263-020-01303-4>.
- D. Van Veen, A. Jalal, M. Soltanolkotabi, E. Price, S. Vishwanath, and A. G. Dimakis. Compressed Sensing with Deep Image Prior and Learned Regularization. jun 2018.

URL <http://arxiv.org/abs/1806.06438>.

- G. Wang, G. B. Giannakis, and Y. C. Eldar. Solving Systems of Random Quadratic Equations via Truncated Amplitude Flow. *arXiv:1605.08285 [cs, math, stat]*, May 2016. URL <http://arxiv.org/abs/1605.08285>.
- K. Zhang, W. Zuo, Y. Chen, D. Meng, and L. Zhang. Beyond a Gaussian Denoiser: Residual Learning of Deep CNN for Image Denoising. *IEEE Transactions on Image Processing*, 26(7):3142–3155, July 2017. ISSN 1057-7149, 1941-0042. doi: 10.1109/TIP.2017.2662206. URL <http://arxiv.org/abs/1608.03981>. arXiv: 1608.03981.